International Journal of Mechanical, Industrial and Aerospace Sciences
ISSN: 2517-9950
Vol:5, No:2, 2011

# Active Fiber Composites for Smart Damping of Doubly Curved Laminated Shells

Saroj Kumar Sarangi and M. C. Ray

***Abstract*****—**This paper deals with the analysis of active constrained layer damping (**ACLD**) of doubly curved laminated composite shells using active fiber composite (**AFC**) materials. The constraining layer of the **ACLD** treatment has been considered to be made of the **AFC** materials. A three dimensional energy based finite element model of the smart doubly curved laminated composite shell integrated with a patch of such **ACLD** treatment has been developed to demonstrate the performance of the patch on enhancing the damping characteristics of the doubly curved laminated composite shells. Particular emphasis has been placed on studying the effect of variation of piezoelectric fiber orientation angle in the constraining **AFC** layer on the control authority of the **ACLD** patch.

***Keywords*****—** Active constrained layer damping, Active fiber composites**,** Finite element modeling, First order shear deformation theory.

## I. Introduction

MONOLITHIC piezoelectric materials have been widely used as distributed sensors and actuators for developing smart structures with self-monitoring and self-controlling capabilities [1]–[12]. However, their major drawback is low control authority as the magnitude of their electromechanical coefficients is very small. To improve the situation, the concept of active constrained layer damping (**ACLD**) treatment was developed [13]. In **ACLD** treatment, a layer of viscoelastic material is constrained between the host structure and a constraining layer made of piezoelectric materials. When the constraining layer is activated by suitable control voltage, the shear deformations of the viscoelastic layer are enhanced thereby improving the damping characteristics of the overall structure. Since its inception, the **ACLD** treatment has gained much importance and wide acceptability for the purpose of efficient and reliable control of flexible structures [14]-[16].

Piezoelectric composites (**PZC**) are now being extensively used as distributed actuators and sensors of smart structures. These **PZC**s are usually composed of an epoxy matrix reinforced with fibers of monolithic piezoelectric materials, provide a wide range of effective material properties not offered by existing monolithic piezoelectric materials, render anisotropic actuations and are characterized by good conformability and strength.

Saroj Kumar Sarangi, PhD Student, is with the Department of Mechanical Engineering, Indian Institute of Technology (IIT), Kharagpur, INDIA, 721302, e-mail: sarojksarangi@yahoo.com

M. C. Ray, Professor, is with the Department of Mechanical Engineering, Indian Institute of Technology (IIT), Kharagpur, INDIA, 721302, e-mail: mcray@mech.iitkgp.ernet.in

One of the commercially available **PZC** is the active fiber composite (**AFC**), developed by Bent and Hagood [17]. A lamina of **AFC** is composed of piezoceramic fibers horizontally aligned in the plane of the lamina while the fibers are poled along their length. The arrangement of electrodes in **AFC** attributes the distributed actuator made of **AFC** with high in-plane actuation authority along the fiber direction. Papers are available on the active vibration control of laminated composite shells [18-21]. From the open literature on active control of smart laminated composite structures, it seems that, the performance of **AFC** material has not yet been studied for the purpose of active control of doubly curved laminated composite shells.

In this paper, the authors intend to investigate the performance of **AFC** material as the material of the constraining layer of the **ACLD** treatment for active control of thin doubly curved laminated composite shells. For such investigation, a three-dimensional analysis of the **ACLD** of thin doubly curved laminated composite shells integrated with a patch of **ACLD** treatment has been carried out by finite element method. The effect of variation of piezoelectric fiber orientation angle in the constraining **AFC** layer on the control authority of the **ACLD** patch has also been investigated.

## II. Finite Element Modeling

Fig. 1 illustrates a doubly curved laminated composite shallow shell composed of $N$ number of orthotropic layers. The curvilinear lengths of the shell are denoted by $a$ and $b$, respectively, while their principal radii of curvatures are $R_1$

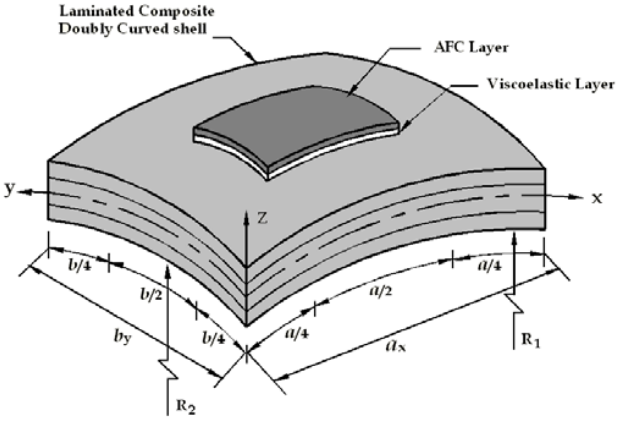


Fig. 1. Schematic representation of a doubly curved laminated composite shell integrated with a patch of **ACLD** treatment composed of active fiber composite (**AFC**) constraining layer.

and $\boldsymbol{R_2}$, respectively. The top surface of the shell is integrated with a rectangular patch of the **ACLD** treatment. The constraining layer of the **ACLD** treatment is made of the **AFC** material and the constrained layer of the treatment is made of a viscoelastic material. The thickness of the constraining layer is $\boldsymbol{h_p}$ and that of the constrained layer is $\boldsymbol{h_v}$. The mid-plane of the substrate shell is considered as the reference plane. As shown in Fig.1, the origin of the curvilinear laminate coordinate system $(\boldsymbol{x, y, z})$ is located at one corner of the reference plane such that the lines $\boldsymbol{x = 0, a}$ and $\boldsymbol{y = 0, b}$ represent the boundary edges of the shell. The thickness co-ordinate $(\boldsymbol{z})$ of the top and bottom surfaces of any layer is denoted by $\boldsymbol{h_{k+1}}$ and $\boldsymbol{h_k}$ , respectively with $\boldsymbol{k}$ denoting the layer number of the layer. The fiber orientation angle in any layer of the substrate shell with respect to the laminate coordinate system is denoted by $\boldsymbol{\theta}$. Since the overall shell considered here is thin, the first order shear deformation theory **(FSDT)** is used to describe the kinematics of deformations of the overall shell integrated with the **ACLD** patch. Fig. 2 describes the schematic representation of the kinematics of deformations based on the **FSDT**. As shown in

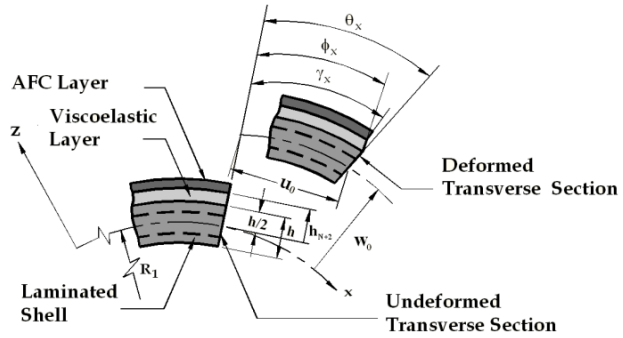


Fig. 2. (a) Deformation of any transverse cross-section of the laminated shell integrated with the **ACLD** treatment which is parallel to the yz- plane.(b) Deformation of any transverse cross-section of the laminated shell integrated with the **ACLD** treatment which is parallel to the xz- plane.

this figure, $\boldsymbol{u_0}$ and $\boldsymbol{v_0}$ are the generalized translational displacements of a point $(\boldsymbol{x, y})$ on the reference plane $(\boldsymbol{z = 0})$ along $\boldsymbol{x}$- and $\boldsymbol{y}$- directions, respectively; $\boldsymbol{\theta_x}$, $\boldsymbol{\Phi_x}$ and $\boldsymbol{\gamma_x}$ are the generalized rotations of the normal to the middle planes of the substrate, the viscoelastic layer and the **AFC** layer, respectively about $\boldsymbol{y}$-axis while the generalized rotations of these normals about $\boldsymbol{x}$-axis are denoted, respectively, by $\boldsymbol{\theta_y}$, $\boldsymbol{\Phi_y}$ and $\boldsymbol{\gamma_y}$. According to the kinematics of deformation as illustrated in Fig.2, the displacements $\boldsymbol{u}$ and $\boldsymbol{v}$ of any point in the domain of the overall shell along $\boldsymbol{x}$- and $\boldsymbol{y}$- directions, respectively, can be written as:

$$\boldsymbol{u(x,y,z,t) = u_0(x,y,t) + \left(z - \langle z - \frac{h}{2}\rangle\right)\theta_x(x,y,t) + \left(\langle z - \frac{h}{2}\rangle - \langle z - h_{N+2}\rangle\right)\Phi_x(x,y,t) + \langle z - h_{N+2}\rangle\gamma_x(x,y,t)} \quad (1)$$

$$\boldsymbol{v(x,y,z,t) = v_0(x,y,t) + \left(z - \langle z - \frac{h}{2}\rangle\right)\theta_y(x,y,t) + \left(\langle z - \frac{h}{2}\rangle - \langle z - h_{N+2}\rangle\right)\Phi_y(x,y,t) + \langle z - h_{N+2}\rangle\gamma_y(x,y,t)} \quad (2)$$

in which a function within the bracket $\langle\ \rangle$ represents the appropriate singularity functions. Similar to the in-plane displacements, the transverse displacement at any point of the overall shell can be written as

$$\boldsymbol{w(x,y,z,t) = w_0(x,y,t) + \left(z - \langle z - \frac{h}{2}\rangle\right)\theta_z(x,y,t) + \left(\langle z - \frac{h}{2}\rangle - \langle z - h_{N+2}\rangle\right)\Phi_z(x,y,t) + \langle z - h_{N+2}\rangle\gamma_z(x,y,t)} \quad (3)$$

where $\mathbf{w_0}$ is the transverse displacement of a point in the reference plane.

For the ease of analysis, the generalized displacement variables are grouped into translational $\{\boldsymbol{d_t}\}$ and rotational $\{\boldsymbol{d_r}\}$ variables as follows:

$$\{\boldsymbol{d_t}\} = [\,\boldsymbol{u_0}\ \ \boldsymbol{v_0}\ \ \boldsymbol{w_0}\,]^T \text{and}$$
$$\{\boldsymbol{d_r}\} = \left[\,\boldsymbol{\theta_x}\ \ \boldsymbol{\theta_y}\ \ \boldsymbol{\theta_z}\ \ \boldsymbol{\Phi_x}\ \ \boldsymbol{\Phi_y}\ \ \boldsymbol{\Phi_z}\ \ \boldsymbol{\gamma_x}\ \ \boldsymbol{\gamma_y}\ \ \boldsymbol{\gamma_z}\,\right]^T \quad (4)$$

In order to implement the selective integration rule in a straight forward manner for avoiding the shear locking in thin structures, the state of strains at any point in the overall shell is represented by the two vectors $\{\boldsymbol{\varepsilon_b}\}$ and $\{\boldsymbol{\varepsilon_s}\}$ and are given by

$$\{\boldsymbol{\varepsilon_b}\} = \left[\boldsymbol{\varepsilon_x}\ \ \boldsymbol{\varepsilon_y}\ \ \boldsymbol{\varepsilon_{xy}}\ \ \boldsymbol{\varepsilon_z}\right]^T \text{ and } \{\boldsymbol{\varepsilon_s}\} = \left[\boldsymbol{\varepsilon_{xz}}\ \ \boldsymbol{\varepsilon_{yz}}\right]^T \quad (5)$$

where, $\boldsymbol{\varepsilon_x}$ , $\boldsymbol{\varepsilon_y}$ and $\boldsymbol{\varepsilon_z}$ are the normal strains along **x-**, **y-** and **z-** directions, respectively; $\boldsymbol{\varepsilon_{xy}}$ is the in-plane shear strain; $\boldsymbol{\varepsilon_{xz}}$ and $\boldsymbol{\varepsilon_{yz}}$ are the transverse shear strains.

By using the displacement field given by Eqs. (1)-(3), the linear strain displacement relations and Eq. (5), the vectors $\{\boldsymbol{\varepsilon_b}\}_c$ , $\{\boldsymbol{\varepsilon_b}\}_v$ and $\{\boldsymbol{\varepsilon_b}\}_p$ defining the state of in-plane and transverse normal strains and the vectors $\{\boldsymbol{\varepsilon_s}\}_c$ , $\{\boldsymbol{\varepsilon_s}\}_v$ and $\{\boldsymbol{\varepsilon_s}\}_p$ defining the state of transverse shear strains at any point in the substrate composite shell, the viscoelastic layer and the **AFC** layer, respectively, can be expressed as

$$\{\boldsymbol{\varepsilon_b}\}_c = \{\boldsymbol{\varepsilon_{bt}}\} + [\boldsymbol{Z_1}]\{\boldsymbol{\varepsilon_{br}}\}, \quad \{\boldsymbol{\varepsilon_b}\}_v = \{\boldsymbol{\varepsilon_{bt}}\} + [\boldsymbol{Z_2}]\{\boldsymbol{\varepsilon_{br}}\},$$
$$\{\boldsymbol{\varepsilon_b}\}_p = \{\boldsymbol{\varepsilon_{bt}}\} + [\boldsymbol{Z_3}]\{\boldsymbol{\varepsilon_{br}}\}, \ \{\boldsymbol{\varepsilon_s}\}_c = \{\boldsymbol{\varepsilon_{st}}\} + [\boldsymbol{Z_4}]\{\boldsymbol{\varepsilon_{sr}}\},$$
$$\{\boldsymbol{\varepsilon_s}\}_v = \{\boldsymbol{\varepsilon_{st}}\} + [\boldsymbol{Z_5}]\{\boldsymbol{\varepsilon_{sr}}\}, \ \{\boldsymbol{\varepsilon_s}\}_p = \{\boldsymbol{\varepsilon_{st}}\} + [\boldsymbol{Z_6}]\{\boldsymbol{\varepsilon_{sr}}\} \quad (6)$$

The various matrices $[\mathbf{Z_1}]$, $[\mathbf{Z_2}]$, $[\mathbf{Z_3}]$, $[\mathbf{Z_4}]$, $[\mathbf{Z_5}]$ and $[\mathbf{Z_6}]$ appearing in Eq.(6) are defined in the **Appendix** while the generalized strain vectors are given by

$$\{\boldsymbol{\varepsilon}_{bt}\} = \left[\frac{\partial \boldsymbol{u_0}}{\partial \boldsymbol{x}} + \frac{\boldsymbol{w}}{\boldsymbol{R_1}} \quad \frac{\partial \boldsymbol{v_0}}{\partial \boldsymbol{y}} + \frac{\boldsymbol{w}}{\boldsymbol{R_2}} \quad \frac{\partial \boldsymbol{u_0}}{\partial \boldsymbol{y}} + \frac{\partial \boldsymbol{v_0}}{\partial \boldsymbol{x}} \quad \boldsymbol{0}\right]^T,$$

$$\{\boldsymbol{\varepsilon}_{br}\} = \begin{bmatrix} \frac{\partial \boldsymbol{\theta_x}}{\partial \boldsymbol{x}} & \frac{\partial \boldsymbol{\theta_y}}{\partial \boldsymbol{y}} & \frac{\partial \boldsymbol{\theta_x}}{\partial \boldsymbol{y}} + \frac{\partial \boldsymbol{\theta_y}}{\partial \boldsymbol{x}} & \boldsymbol{\theta_z} & \frac{\partial \boldsymbol{\Phi_x}}{\partial \boldsymbol{x}} & \frac{\partial \boldsymbol{\Phi_y}}{\partial \boldsymbol{y}} \\ \frac{\partial \boldsymbol{\Phi_x}}{\partial \boldsymbol{y}} + \frac{\partial \boldsymbol{\Phi_y}}{\partial \boldsymbol{x}} & \boldsymbol{\Phi_z} & \frac{\partial \boldsymbol{\gamma_x}}{\partial \boldsymbol{x}} & \frac{\partial \boldsymbol{\gamma_y}}{\partial \boldsymbol{y}} & \frac{\partial \boldsymbol{\gamma_x}}{\partial \boldsymbol{y}} + \frac{\partial \boldsymbol{\gamma_y}}{\partial \boldsymbol{x}} & \boldsymbol{\gamma_z} \end{bmatrix}^T,$$

$$\{\boldsymbol{\varepsilon}_{st}\} = \left[\frac{\partial \boldsymbol{w_0}}{\partial \boldsymbol{x}} - \frac{\boldsymbol{u_0}}{\boldsymbol{R_1}} \quad \frac{\partial \boldsymbol{w_0}}{\partial \boldsymbol{y}} - \frac{\boldsymbol{v_0}}{\boldsymbol{R_2}}\right]^T,$$

$$\{\boldsymbol{\varepsilon}_{sr}\} = \begin{bmatrix} \boldsymbol{\theta_x} & \boldsymbol{\theta_y} & \boldsymbol{\Phi_x} & \boldsymbol{\Phi_y} & \boldsymbol{\gamma_x} & \boldsymbol{\gamma_y} \\ \frac{\partial \boldsymbol{\theta_z}}{\partial \boldsymbol{x}} & \frac{\partial \boldsymbol{\theta_z}}{\partial \boldsymbol{y}} & \frac{\partial \boldsymbol{\Phi_z}}{\partial \boldsymbol{x}} & \frac{\partial \boldsymbol{\Phi_z}}{\partial \boldsymbol{y}} & \frac{\partial \boldsymbol{\gamma_z}}{\partial \boldsymbol{x}} & \frac{\partial \boldsymbol{\gamma_z}}{\partial \boldsymbol{y}} \end{bmatrix}^T \quad (7)$$

Corresponding to the description of the state of strains given by Eq. (5), the state of stresses at any point in the overall shell can be expressed as,

$\{\boldsymbol{\sigma_b}\} = \left[\boldsymbol{\sigma_x} \quad \boldsymbol{\sigma_y} \quad \boldsymbol{\sigma_{xy}} \quad \boldsymbol{\sigma_z}\right]^T$ and $\{\boldsymbol{\sigma_s}\} = \left[\boldsymbol{\sigma_{xz}} \quad \boldsymbol{\sigma_{yz}}\right]^T$ (8)

where $\sigma_x$, $\sigma_y$ and $\sigma_z$ are the normal stresses along x-, y- and z-directions respectively; $\sigma_{xy}$ is the in plane shear stress; $\sigma_{xz}$ and $\sigma_{yz}$ are the transverse shear stresses.

The constitutive relations for the material of orthotropic layers of the host shell are given by

$\{\sigma_b^k\} = [\bar{C}_b^k]\{\varepsilon_b^k\}$ and $\{\sigma_s^k\} = [\bar{C}_s^k]\{\varepsilon_s^k\},\ k = 1,2,3,\dots,N$ (9)

where $[\overline{\boldsymbol{C}}_{\boldsymbol{b}}^{\boldsymbol{k}}] = \begin{bmatrix} \overline{\boldsymbol{C}}_{\boldsymbol{11}}^{\boldsymbol{k}} & \overline{\boldsymbol{C}}_{\boldsymbol{12}}^{\boldsymbol{k}} & \overline{\boldsymbol{C}}_{\boldsymbol{16}}^{\boldsymbol{k}} & \overline{\boldsymbol{C}}_{\boldsymbol{13}}^{\boldsymbol{k}} \\ \overline{\boldsymbol{C}}_{\boldsymbol{12}}^{\boldsymbol{k}} & \overline{\boldsymbol{C}}_{\boldsymbol{22}}^{\boldsymbol{k}} & \overline{\boldsymbol{C}}_{\boldsymbol{26}}^{\boldsymbol{k}} & \overline{\boldsymbol{C}}_{\boldsymbol{23}}^{\boldsymbol{k}} \\ \overline{\boldsymbol{C}}_{\boldsymbol{16}}^{\boldsymbol{k}} & \overline{\boldsymbol{C}}_{\boldsymbol{26}}^{\boldsymbol{k}} & \overline{\boldsymbol{C}}_{\boldsymbol{66}}^{\boldsymbol{k}} & \overline{\boldsymbol{C}}_{\boldsymbol{36}}^{\boldsymbol{k}} \\ \overline{\boldsymbol{C}}_{\boldsymbol{13}}^{\boldsymbol{k}} & \overline{\boldsymbol{C}}_{\boldsymbol{23}}^{\boldsymbol{k}} & \overline{\boldsymbol{C}}_{\boldsymbol{36}}^{\boldsymbol{k}} & \overline{\boldsymbol{C}}_{\boldsymbol{33}}^{\boldsymbol{k}} \end{bmatrix}$, $[\overline{\boldsymbol{C}}_{\boldsymbol{s}}^{\boldsymbol{k}}] = \begin{bmatrix} \overline{\boldsymbol{C}}_{\boldsymbol{55}}^{\boldsymbol{k}} & \overline{\boldsymbol{C}}_{\boldsymbol{45}}^{\boldsymbol{k}} \\ \overline{\boldsymbol{C}}_{\boldsymbol{45}}^{\boldsymbol{k}} & \overline{\boldsymbol{C}}_{\boldsymbol{44}}^{\boldsymbol{k}} \end{bmatrix}$

Assuming that the viscoelastic layer is linear and isotropic, its shear modulus $\boldsymbol{G}$ and the Young's modulus $\boldsymbol{E}$ can be represented as [14]

$\boldsymbol{G} = \boldsymbol{G}'(\boldsymbol{1} + \boldsymbol{i\eta})$ and $\boldsymbol{2G(1+\upsilon)}$ (10)

where $\boldsymbol{G}'$ is the storage modulus, $\boldsymbol{\upsilon}$ is the Poisson's ratio and $\boldsymbol{\eta}$ is the loss factor at a particular operating temperature and frequency. Employing the complex modulus approach, the constitutive relations for the material of the viscoelastic layer $(\boldsymbol{k = N+1})$ can also be represented by Eq. (9) with $\overline{\boldsymbol{C}}_{\boldsymbol{ij}}^{\boldsymbol{N+1}}\ (\boldsymbol{i,j = 1,2,3,\dots,6})$ being the complex elastic constants.

In the present work, the electric field $\boldsymbol{E_x}$ is applied in the **x** direction and the constitutive equations for the **AFC** material are expressed as

$\{\sigma_b^k\} = [\bar{C}_b^k]\{\epsilon_b^k\} - \{e_b^k\}E_x$, $\{\sigma_s^k\} = [\bar{C}_s^k]\{\epsilon_s^k\}$

and $D_z = \{e_b^k\}^{\mathrm{T}}\{\epsilon_b^k\} + \bar{\epsilon}_{11}E_x$ (11)

in which the piezoelectric coefficient matrix $\{e_b^k\}$ is given by $\{e_b^k\} = [\bar{e}_{11} \quad \bar{e}_{12} \quad \bar{e}_{13} \quad \bar{e}_{16}]^T$ and $\bar{\epsilon}_{11}$ is the transformed dielectric constant of the **AFC** material. Also, the electric field $E_x$ is given by $E_x = -V/d_p$ with $d_p$ and $V$ being the distance between the positive and the negative electrodes and the applied voltage difference between these electrodes, respectively.

The principle of virtual work is employed to derive the governing equations of motion of the overall shell/**ACLD** system and can be expressed as

$$\sum_{k=1}^{N+2}\int_{\Omega}\left(\delta\{\in_b^k\}^T\{\sigma_b^k\} + \delta\{\in_s^k\}^T\{\sigma_s^k\} - \delta E_x\bar{\varepsilon}_{33}E_x - \delta\{d_t\}^T\rho^k\{\ddot{d}_t\}\right)d\Omega - \int_A \delta\{d_t\}^T\{f\}dA = 0 \quad (12)$$

in which $\boldsymbol{\rho^k}$ is the mass density of the $\boldsymbol{k^{th}}$ layer, $\{\boldsymbol{f}\}$ is the externally applied surface traction acting over a surface area $\boldsymbol{A}$ and $\boldsymbol{\Omega}$ represents the volume of the concerned layer. Since the shell under study is considered to be thin, the rotary inertia of the overall shell has been neglected in estimating the kinetic energy. The overall shell is discretized by eight noded isoparametric quadrilateral elements. Thus following Eq. (4), the generalized displacement vectors for the $\mathbf{i}^{\text{th}}$ $(\boldsymbol{i = 1,2,3,\dots,8})$ node of the element can be denoted as

$\{\boldsymbol{d}_{ti}\} = [\ \boldsymbol{u_{0i}}\ \ \boldsymbol{v_{0i}}\ \ \boldsymbol{w_{0i}}\ ]^T$ and

$\{\boldsymbol{d}_{ri}\} = \left[\ \boldsymbol{\theta_{xi}}\ \ \boldsymbol{\theta_{yi}}\ \ \boldsymbol{\theta_{zi}}\ \ \boldsymbol{\Phi_{xi}}\ \ \boldsymbol{\Phi_{yi}}\ \ \boldsymbol{\Phi_{z\,i}}\ \ \boldsymbol{\gamma_{xi}}\ \ \boldsymbol{\gamma_{yi}}\ \ \boldsymbol{\gamma_{zi}}\ \right]^T$ (13)

The generalized displacement vectors at any point within the element can be written as

$\{\boldsymbol{d_t}\} = [\boldsymbol{N_t}]\{\boldsymbol{d_t^e}\}$ and $\{\boldsymbol{d_r}\} = [\boldsymbol{N_r}]\{\boldsymbol{d_r^e}\}$ (14)

in which the shape function matrices $[\mathbf{N_t}]$, $[\mathbf{N_r}]$ and the nodal generalized displacement vectors $\{\boldsymbol{d_t^e}\}$ and $\{\boldsymbol{d_r^e}\}$ are given by

$[\mathbf{N_t}] = [\mathbf{N_{t1}} \quad \mathbf{N_{t2}} \ \dots \ \mathbf{N_{t8}}]^{\mathbf{T}}$,

$[\mathbf{N_r}] = [\mathbf{N_{r1}} \quad \mathbf{N_{r2}} \ \dots \ \mathbf{N_{r8}}]^{\mathbf{T}}$, $\mathbf{N_{ti}} = \mathbf{n_i I_t}$, $\mathbf{N_{ri}} = \mathbf{n_i I_r}$,

$\{\boldsymbol{d_t^e}\} = [\{\boldsymbol{d_{t1}^e}\}^T \quad \{\boldsymbol{d_{t2}^e}\}^T \ \dots \ \{\boldsymbol{d_{t8}^e}\}^T]^T$ and

$\{\boldsymbol{d_r^e}\} = [\{\boldsymbol{d_{r1}^e}\}^T \quad \{\boldsymbol{d_{r2}^e}\}^T \ \dots \ \{\boldsymbol{d_{r8}^e}\}^T]^T$ (15)

with $\boldsymbol{I_t}$ and $\boldsymbol{I_r}$ being the 3 × 3 and 9 × 9 identity matrices, respectively and $\boldsymbol{n_i}$ the shape functions of natural coordinates associated with the $\mathbf{i}^{\text{th}}$ node. Using the relations given by Eq.(15) in Eq.(6), the generalized strain vectors at any point within the element can be expressed as follows:

$\{\boldsymbol{\varepsilon_{bt}}\} = [\boldsymbol{B_{tb}}]\{\boldsymbol{d_t^e}\}$ , $\{\boldsymbol{\varepsilon_{br}}\} = [\boldsymbol{B_{rb}}]\{\boldsymbol{d_r^e}\}$ ,

$\{\boldsymbol{\varepsilon_{st}}\} = [\boldsymbol{B_{ts}}]\{\boldsymbol{d_t^e}\}$ , $\{\boldsymbol{\varepsilon_{sr}}\} = [\boldsymbol{B_{rs}}]\{\boldsymbol{d_r^e}\}$ (16)

in which the nodal strain-displacement matrices $[\boldsymbol{B_{tb}}]$, $[\boldsymbol{B_{rb}}]$, $[\boldsymbol{B_{ts}}]$ and $[\boldsymbol{B_{rs}}]$ are given by

$[\boldsymbol{B_{tb}}] = [\boldsymbol{B_{tb1}} \quad \boldsymbol{B_{tb2}} \ \dots \ \boldsymbol{B_{tb8}}]$,

$[\boldsymbol{B_{rb}}] = [\boldsymbol{B_{rb1}} \quad \boldsymbol{B_{rb2}} \ \dots \ \boldsymbol{B_{rb8}}]$,

$[\boldsymbol{B_{ts}}] = [\boldsymbol{B_{ts1}} \quad \boldsymbol{B_{ts2}} \ \dots \ \boldsymbol{B_{ts8}}]$ and

$[\boldsymbol{B_{rs}}] = [\boldsymbol{B_{rs1}} \quad \boldsymbol{B_{rs2}} \ \dots \ \boldsymbol{B_{rs8}}]$ (17)

The various submatrices appearing in Eq. (17) are explained in the **Appendix.** On substitution of Eqs. (14) and (16) into Eq. (12), one can derive the following open loop equations of motion of an element integrated with the **ACLD** treatment:

$[\boldsymbol{M^e}]\{\ddot{\boldsymbol{d}}_{\boldsymbol{t}}^{\boldsymbol{e}}\} + [\boldsymbol{K_{tt}^e}]\{\boldsymbol{d_t^e}\} + [\boldsymbol{K_{tr}^e}]\{\boldsymbol{d_r^e}\} = \{\boldsymbol{F_{tp}^e}\}\boldsymbol{V} + \{\boldsymbol{F^e}\}$ (18)

$[\boldsymbol{K_{tr}^e}]^T\{\boldsymbol{d_t^e}\} + [\boldsymbol{K_{rr}^e}]\{\boldsymbol{d_r^e}\} = \{\boldsymbol{F_{rp}^e}\}\boldsymbol{V}$ (19)

The elemental stiffness matrices ($[\boldsymbol{K_{tt}^e}]$,$[\boldsymbol{K_{tr}^e}]$,$[\boldsymbol{K_{rr}^e}]$), the elemental electro-elastic coupling vectors ($\{\boldsymbol{F_{tp}^e}\}$, $\{\boldsymbol{F_{rp}^e}\}$), the elemental load vector $\{\boldsymbol{F^e}\}$ and the elemental mass matrix $[\boldsymbol{M^e}]$ appearing in Eqs. (18) and (19) are derived as follows:

$[\boldsymbol{K_{tt}^e}] = [\boldsymbol{K_{tb}^e}] + [\boldsymbol{K_{ts}^e}]$, $[\boldsymbol{K_{tr}^e}] = [\boldsymbol{K_{trb}^e}] + [\boldsymbol{K_{trs}^e}]$,

$[\boldsymbol{K_{rr}^e}] = [\boldsymbol{K_{rrb}^e}] + [\boldsymbol{K_{rrs}^e}]$,

$$[K^e_{tb}] = \int_0^{b_e}\int_0^{a_e} [B_{tb}]^T [D_{tb}][B_{tb}]\, dx\, dy,$$
$$[K^e_{ts}] = \int_0^{b_e}\int_0^{a_e} [B_{ts}]^T [D_{ts}][B_{ts}]\, dx\, dy,$$
$$[K^e_{trb}] = \int_0^{b_e}\int_0^{a_e} [B_{tb}]^T [D_{trb}][B_{rb}]\, dx\, dy,$$
$$[K^e_{trs}] = \int_0^{b_e}\int_0^{a_e} [B_{ts}]^T [D_{trs}][B_{rs}]\, dx\, dy,$$
$$[K^e_{rrb}] = \int_0^{b_e}\int_0^{a_e} [B_{rb}]^T [D_{rrb}][B_{rb}]\, dx\, dy,$$
$$[K^e_{rrs}] = \int_0^{b_e}\int_0^{a_e} [B_{rs}]^T [D_{rrs}][B_{rs}]\, dx\, dy,$$
$$[F^e_{tp}] = \int_0^{b_e}\int_0^{a_e} [B_{tb}]^T [F_{tbp}]\, dx\, dy,$$
$$[F^e_{rp}] = \int_0^{b_e}\int_0^{a_e} [B_{rb}]^T [F_{rbp}]\, dx\, dy,$$
$$[M^e] = \int_0^{b_e}\int_0^{a_e} \bar{m}\ [N_t]^T[N_t] dx\, dy\,,$$
$$\bar{m} = \sum_{k=1}^{N=2}\int_{h_k}^{h_{k+1}} \rho^k\, dz \qquad (20)$$

where $a_e$ and $b_e$ are the circumferential length and the circumferential width of the element under consideration and the various rigidity matrices originated in the above elemental matrices are given in the **Appendix.**

Since the elastic constant matrix of the viscoelastic layer is complex, the stiffness matrices of an element integrated with the **ACLD** treatment are complex. For an element without integrated with the **ACLD** treatment, the electro-elastic coupling matrices become null vectors and the elemental stiffness matrices will be real. Finally, the elemental equations of motion are assembled to obtain the open loop global equation of motion of the overall shell integrated with the **ACLD** patch as follows:

$$[M]\{\ddot{X}\} + [K_{tt}]\{X\} + [K_{tr}]\{X_r\} = \{F_{tp}\}V + \{F\} \qquad (21)$$
$$[K_{tr}]^T\{X\} + [K_{rr}]\{X_r\} = \{F_{rp}\}V \qquad (22)$$

where $[M]$ is the global mass matrix, $[K_{tt}]$, $[K_{tr}]$ and $[K_{rr}]$ are the global stiffness matrices, $\{F_{tp}\}$, $\{F_{rp}\}$ are the global electro-elastic coupling vectors, $\{X\}$ and $\{X_r\}$ are the global nodal generalized displacement vectors, $\{F\}$ is the global nodal force vector and $V$ is the voltage applied to the constraining layer of the **ACLD** patch. Because of the complex elemental stiffness matrices of an element augmented with the **ACLD** treatment, the global stiffness matrices turn out to be complex and the energy dissipation characteristics of the overall shell is attributed to the imaginary part of these matrices. Hence, the global equations of motion as derived above also represent the passive (uncontrolled) constrained layer damping of the substrate shell when the constraining layer is not subjected to any control voltage.

## III. CLOSED LOOP MODEL

The active constraining layer of the **ACLD** patch is activated with a control voltage proportional to the transverse velocity of a point. Thus the control voltage can be expressed in terms of the derivatives of the global nodal degrees of freedom as follows:

$$V = -K_d\, \dot{w} = -K_d[U]\{\dot{X}\} \qquad (23)$$

in which $K_d$ is the control gain and $[U]$ is a unit vector defining the location of sensing the velocity signal that will be fed back to the **ACLD** patch.

Substituting Eq. (23) into Eqs. (21) and (22), the final equations of motion governing the closed loop dynamics of the overall shell/**ACLD** system can be obtained as follows:

$$[M]\{\ddot{X}\} + [K_{tt}]\{X\} + [K_{tr}]\{X_r\} + K_d\{F_{tp}\}[U]\{\dot{X}\} = \{F\} \qquad (24)$$
$$[K_{tr}]^T\{X\} + [K_{rr}]\{X_r\} + K_d\{F_{rp}\}[U]\{\dot{X}\} = 0 \qquad (25)$$

## IV. RESULTS AND DISCUSSIONS

In this Section, numerical results are computed using the finite element model derived in the previous section to assess the performance of the **ACLD** patch for causing active damping of doubly curved laminated composite shells. Symmetric and antisymmetric cross-ply thin shallow shells integrated with a rectangular patch of **ACLD** treatment (Fig. 1) are considered as the numerical examples. The material properties for the orthotropic layers of the substrate shell are considered as follows:

$E_L = 172\ GPa,\ E_L/E_T = 25,\ G_{LT} = 0.5\ E_T,$
$G_{TT} = 0.2\ E_T,\ \nu_{LT} = \nu_{TT} = 0.25, \rho = 1600\ kg/m^3$

in which the symbols have their usual meaning [22]. Also, the effective material properties of the **AFC** material obtained from [23] are used here for evaluating the numerical results.

$C_{11} = 138.1\ GPa,\ C_{12} = 71.15\ GPa,\ C_{22} = 148.9\ GPa,$
$C_{44} = C_{55} = 32.35\ GPa, C_{66} = 39.14\ GPa,$
$e_{11} = 14.14\ C/m^2,\ e_{12} = e_{13} - 3.34\ C/m^2,\ e_{16} = 0$

The thicknesses of the **AFC** layer, the viscoelastic layer and the laminated shell are considered as 250 **μm**, 50.8 **μm** and 3 **mm** respectively, while the orthotropic layers of the substrate shell are of equal thickness. The shells are having square plan form where $a_x = b_y = 1\ m$ (Fig.1) and the radius of curvature $R_2$ is taken as $300\ h$. The circumferential length ($a$) and the circumferential width ($b$) of the shell are determined using the standard geometrical relations and unless otherwise mentioned, the radii of curvature $R_1$ and $R_2$ are considered to be same. The length and the width of the **ACLD** patch are assumed to be half of the outer circumferential length and width of the shell, respectively (Fig.1). The simply supported boundary conditions at the edges of the overall shell considered for evaluating the numerical results are given by

$v_0 = w_0 = \theta_y = \theta_z = \Phi_y = \Phi_z = \gamma_y = \gamma_z = 0$ at $x = 0, a$
$u_0 = w_0 = \theta_x = \theta_z = \Phi_x = \Phi_z = \gamma_x = \gamma_z = 0$ at $y = 0, b$

In order to verify the validity of the present finite element model, the non-dimensional fundamental frequencies of the laminated shell integrated with the inactivated **ACLD** patch of negligible thickness are first computed and subsequently compared with the existing results [24] of the identical shells without integrated with the patch. Table 1 illustrates this comparison. The non-dimensional frequency parameter $\bar{\omega}$

used for a particular shell has been considered according to the reference shown in Table 1 with which the present results for

TABLE I
NON-DIMENSIONAL FUNDAMENTAL FREQUENCIES OF LAMINATED CROSS-PLY ($0^0/90^0/0^0$) SHALLOW SHELLS ($R_1 = R_1 = R$) WITH NEGLIGIBLE THICKNESS OF ACLD PATCH.

| $R/a$ | $\bar{\omega}$ * | | | |
|---|---|---|---|---|
| | $a/h$=10 | | $a/h$=100 | |
| | Ref. [24] | Present | Ref. [24] | Present |
| 5 | 12.372 | 12.361 | 30.993 | 30.306 |
| 10 | 12.215 | 12.201 | 20.347 | 20.175 |
| 20 | 12.176 | 12.13 | 16.627 | 16.218 |
| 50 | 12.165 | 12.118 | 15.424 | 15.176 |

*$\bar{\omega} = \omega(a^2/h)\sqrt{\rho/E_T}$, $\omega$ is the circular natural frequency

that shell are compared. It may be observed that the results are in excellent agreement validating the model derived here.

Using Eqs. (24) and (25), frequency response functions are computed to study the open loop and closed loop behavior of the overall shell/**ACLD** system. For all frequency response functions presented in this Section, the substrate shells are excited by a transverse harmonic point load of 1 N acting at the point $(a/2, b/4, h/2)$. The control voltage supplied to the constraining layer of the **ACLD** patch is proportional to the velocity of a point $(a/2, b/2, h/2)$. Figs. 3 and 4 illustrate the frequency response functions of the overall shell/**ACLD** systems when the substrates are symmetric and antisymmetric cross-ply spherical ($R_1 = R_2$) shells, respectively. The control gain ($K_d$) is chosen arbitrarily so that the first few modes of vibration are appreciably under control. It may be observed

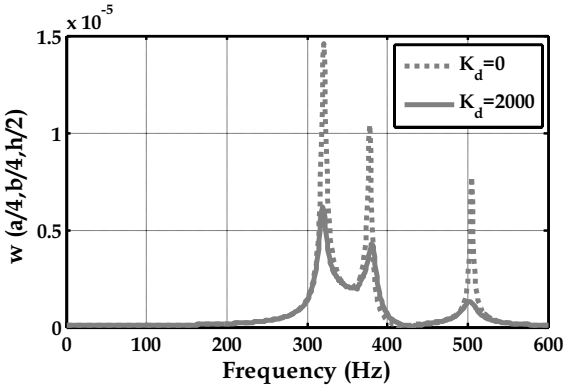


Fig. 3. Frequency response functions for the transverse displacement w of a simply supported symmetric cross-ply ($0^0/90^0/0^0$) spherical ($R_1 = R_2$) shallow shell.

from Figs. 3 and 4 that the active constraining layer made of **AFC** material significantly enhances the damping characteristics of the laminated composite shallow shells. The maximum control voltages required to obtain the controlled responses are also nominal and illustrated in Fig. 5.

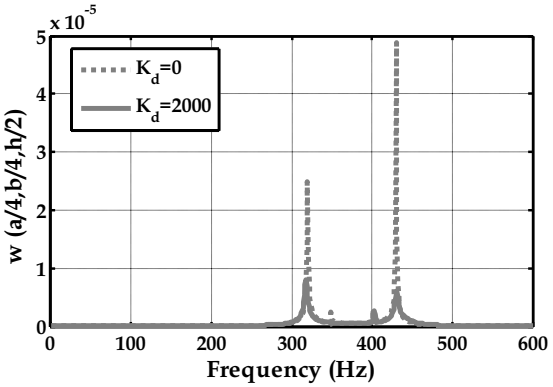


Fig. 4. Frequency response functions for the transverse displacement w of a simply supported antisymmetric cross-ply ($0^0/90^0/0^0/90^0$) spherical ($R_1 = R_2$) shallow shell.

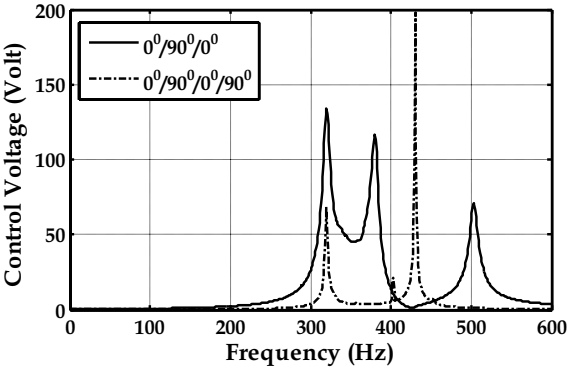


Fig. 5. Control voltage requirements for the active damping of simply supported symmetric and antisymmetric cross-ply spherical ($R_1 = R_2$) shallow shells.

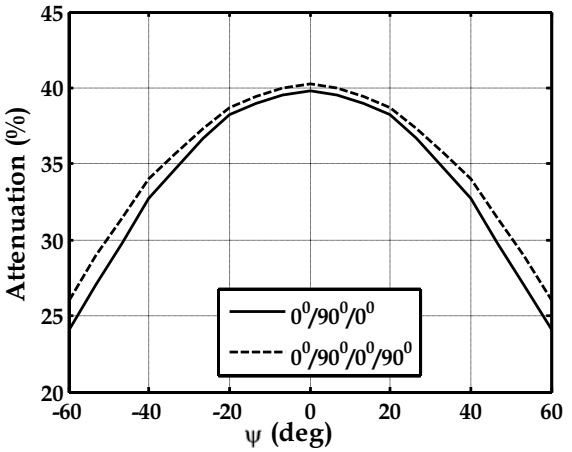


Fig. 6. Effect of variation of the piezoelectric fiber orientation angle in the **AFC** constraining layer of the **ACLD** patch when the fibers are coplanar with the $xy$-plane ($R_1/R_2 = 1$, $\max(V) = 150\ Volt$).

In order to investigate the effects of variation of fiber orientation angle (Ψ) in the constraining **AFC** layer of the **ACLD** patch on enhancing the damping characteristics of thin shells, the percentage attenuation of vibration of the shells are computed with different values of the piezoelectric fiber orientation angle (Ψ) using a particular value of control voltage **(**max (V) =150 Volt). Percentage attenuation of the amplitude is determined with respect to the uncontrolled amplitude of vibration and may be an index for assessing the control authority of the **ACLD** patch. Only the fundamental mode (1, 1) of vibration has been targeted for investigating the attenuating capability of the patch. Fig. 6 demonstrates the effect of variation of the piezoelectric fiber orientation angle in the **AFC** constraining layer on the control authority of the **ACLD** patch for the symmetric and antisymmetric cross-ply laminated shells. It can be clearly observed from this figure that the value of piezoelectric fiber orientation angle should be $\mathbf{0^0}$ for optimum performance of the patch, as shown, for the case of symmetric and antisymmetric cross-ply laminated shells.

## V.CONCLUSIONS

A three dimensional finite element model has been developed to describe the dynamics of doubly curved laminated composite shells integrated with a patch of **ACLD** treatment. The constraining layer of the **ACLD** treatment is considered to be of **AFC** material. Symmetric and antisymmetric cross-ply laminated composite shells integrated with a patch of **ACLD** treatment are considered for evaluation of numerical results. The frequency responses of the shells integrated with the **ACLD** patch, whose constraining layer is made of **AFC** material, illustrate significant enhancement of the active ($\boldsymbol{K_d \neq 0}$) damping characteristics of the shells over the passive ($\boldsymbol{K_d = 0}$) damping. The analyses revealed that the **AFC** material, which is commercially available, may be efficiently used for the constraining layer of the **ACLD** treatment for improving the active damping characteristics of the smart laminated composite shells. It is important to note that the variation of the orientation angle of the piezoelectric fibers of the constraining layer in the $\boldsymbol{xy}$ plane significantly affects the performance of the patch. For optimum performance of the **ACLD** patch, the constraining layer of the patch should be made of **AFC** material having piezofiber orientation angle $\mathbf{0^0}$ with the $\boldsymbol{x}$- direction to attenuate the first mode of the simply supported symmetric and antisymmetric cross-ply shells.

## APPENDIX

The various matrices $[\mathbf{Z_1}]$, $[\mathbf{Z_2}]$, $[\mathbf{Z_3}]$, $[\mathbf{Z_4}]$, $[\mathbf{Z_5}]$ and $[\mathbf{Z_6}]$ appearing in Eq. (6) are given by

$$[\mathbf{Z_1}] = [[\bar{\mathbf{Z}}_1] \quad \tilde{\mathbf{O}} \quad \tilde{\mathbf{O}}], \quad [\mathbf{Z_2}] = \left[\tfrac{\mathbf{h}}{2}[\mathbf{I}] \quad [\bar{\mathbf{Z}}_2] \quad \tilde{\mathbf{O}}\right],$$

$$[\mathbf{Z_3}] = \left[\tfrac{\mathbf{h}}{2}[\mathbf{I}] \quad \mathbf{h_v}[\mathbf{I}] \quad [\bar{\mathbf{Z}}_3]\right],$$

$$[\mathbf{Z_4}] = [[\bar{\mathbf{Z}}_4] \quad \bar{\mathbf{O}} \quad \bar{\mathbf{O}} \quad \mathbf{z}\,\bar{\mathbf{I}} \quad \bar{\mathbf{O}} \quad \bar{\mathbf{O}}],$$

$$[\mathbf{Z_5}] = \left[-(\mathbf{h}/2)\mathbf{I_1} \quad [\bar{\mathbf{Z}}_5] \quad \bar{\mathbf{O}} \quad \tfrac{\mathbf{h}}{2}\,\bar{\mathbf{I}} \quad \left(\mathbf{z}-\tfrac{\mathbf{h}}{2}\right)\bar{\mathbf{I}} \quad \bar{\mathbf{O}}\right],$$

$$[\mathbf{Z_6}] = \left[-(\mathbf{h}/2)\mathbf{I_1} \quad -\mathbf{h_v}\mathbf{I_1} \quad [\bar{\mathbf{Z}}_6] \quad \tfrac{\mathbf{h}}{2}\,\bar{\mathbf{I}} \quad \mathbf{h_v}\bar{\mathbf{I}} \quad (\mathbf{z}-\mathbf{h_{N+2}})\bar{\mathbf{I}}\right]$$

where $[\bar{\mathbf{Z}}_1] = \begin{bmatrix} \mathbf{z}\tilde{\mathbf{I}} & \mathbf{z}[\mathbf{I_2}] \\ \mathbf{O_1} & \mathbf{1} \end{bmatrix}$, $[\bar{\mathbf{Z}}_2] = \begin{bmatrix} (\mathbf{z}-\frac{\mathbf{h}}{2})\tilde{\mathbf{I}} & (\mathbf{z}-\frac{\mathbf{h}}{2})[\mathbf{I_2}] \\ \mathbf{O_1} & \mathbf{1} \end{bmatrix}$,

$[\bar{\mathbf{Z}}_3] = \begin{bmatrix} (\mathbf{z}-\mathbf{h_{N+2}})\tilde{\mathbf{I}} & (\mathbf{z}-\mathbf{h_{N+2}})[\mathbf{I_2}] \\ \mathbf{O_1} & \mathbf{1} \end{bmatrix}$,

$[\bar{\mathbf{Z}}_4] = \begin{bmatrix} \mathbf{1}-(\mathbf{z}/\mathbf{R_1}) & \mathbf{0} \\ \mathbf{0} & \mathbf{1}-(\mathbf{z}/\mathbf{R_2}) \end{bmatrix}$,

$[\bar{\mathbf{Z}}_5] = \begin{bmatrix} \mathbf{1}-(\mathbf{z}-\frac{\mathbf{h}}{2})/\mathbf{R_1} & \mathbf{0} \\ \mathbf{0} & \mathbf{1}-(\mathbf{z}-\frac{\mathbf{h}}{2})/\mathbf{R_2} \end{bmatrix}$,

$[\bar{\mathbf{Z}}_6] = \begin{bmatrix} \mathbf{1}-(\mathbf{z}-\mathbf{h_{N+2}})/\mathbf{R_1} & \mathbf{0} \\ \mathbf{0} & \mathbf{1}-(\mathbf{z}-\mathbf{h_{N+2}})/\mathbf{R_2} \end{bmatrix}$,

$[\mathbf{I}] = \begin{bmatrix} \tilde{\mathbf{I}} & [\mathbf{I_2}] \\ \mathbf{O_1} & \mathbf{0} \end{bmatrix}$, $\mathbf{I_1} = \begin{bmatrix} \mathbf{1/R_1} & \mathbf{0} \\ \mathbf{0} & \mathbf{1/R_2} \end{bmatrix}$

and $[\mathbf{I_2}] = [\mathbf{1/R_1} \quad \mathbf{1/R_2} \quad \mathbf{0}]^{\mathbf{T}}$

$\tilde{\mathbf{O}}$, $\bar{\mathbf{O}}$ and $\mathbf{O_1}$ being 4x4, 2x2 and 1x3 null matrices respectively and $\tilde{\mathbf{I}}$ and $\bar{\mathbf{I}}$ are 3x3 and 2x2 identity matrices respectively.

The various submatrices appearing in Eq. (17) are explained as follows:

$$\boldsymbol{B_{tbi}} = \begin{bmatrix} \frac{\partial n_i}{\partial x} & 0 & \frac{1}{R_1} \\ 0 & \frac{\partial n_i}{\partial y} & \frac{1}{R_2} \\ \frac{\partial n_i}{\partial y} & \frac{\partial n_i}{\partial x} & 0 \\ 0 & 0 & 0 \end{bmatrix}, \quad \boldsymbol{B_{rbi}} = \begin{bmatrix} \bar{\boldsymbol{B}}_{rbi} & \bar{\boldsymbol{O}}_1 & \bar{\boldsymbol{O}}_1 \\ \bar{\boldsymbol{O}}_1 & \bar{\boldsymbol{B}}_{rbi} & \bar{\boldsymbol{O}}_1 \\ \bar{\boldsymbol{O}}_1 & \bar{\boldsymbol{O}}_1 & \bar{\boldsymbol{B}}_{rbi} \end{bmatrix},$$

$$\bar{\boldsymbol{B}}_{rbi} = \begin{bmatrix} \frac{\partial n_i}{\partial x} & 0 & 0 \\ 0 & \frac{\partial n_i}{\partial y} & 0 \\ \frac{\partial n_i}{\partial y} & \frac{\partial n_i}{\partial x} & 0 \\ 0 & 0 & 1 \end{bmatrix}, \boldsymbol{B_{tsi}} = \begin{bmatrix} 0 & -\frac{1}{R_1} & \frac{\partial n_i}{\partial x} \\ 0 & -\frac{1}{R_2} & \frac{\partial n_i}{\partial y} \end{bmatrix}$$

$$\boldsymbol{B_{rsi}} = \begin{bmatrix} \bar{\boldsymbol{I}}_1 \\ \bar{\boldsymbol{B}}_{rsi} \end{bmatrix}, \bar{\boldsymbol{I}}_1 = \begin{bmatrix} \hat{\boldsymbol{I}}_1 & \tilde{\boldsymbol{O}}_1 & \tilde{\boldsymbol{O}}_1 \\ \tilde{\boldsymbol{O}}_1 & \hat{\boldsymbol{I}}_1 & \tilde{\boldsymbol{O}}_1 \\ \tilde{\boldsymbol{O}}_1 & \tilde{\boldsymbol{O}}_1 & \hat{\boldsymbol{I}}_1 \end{bmatrix}, \hat{\boldsymbol{I}}_1 = \begin{bmatrix} 1 & 0 & 0 \\ 0 & 1 & 0 \end{bmatrix}$$

$$\bar{\boldsymbol{B}}_{rsi} = \begin{bmatrix} \tilde{\boldsymbol{B}}_{rsi} & \tilde{\boldsymbol{O}}_1 & \tilde{\boldsymbol{O}}_1 \\ \tilde{\boldsymbol{O}}_1 & \tilde{\boldsymbol{B}}_{rsi} & \tilde{\boldsymbol{O}}_1 \\ \tilde{\boldsymbol{O}}_1 & \tilde{\boldsymbol{O}}_1 & \tilde{\boldsymbol{B}}_{rsi} \end{bmatrix} \text{ and } \tilde{\boldsymbol{B}}_{rsi} = \begin{bmatrix} 0 & 0 & \frac{\partial n_i}{\partial x} \\ 0 & 0 & \frac{\partial n_i}{\partial y} \end{bmatrix}$$

where $\tilde{\boldsymbol{O}}_1$ and $\bar{\boldsymbol{O}}_1$ are (4×3) and (2×3) null matrices, respectively.

The various rigidity matrices originated in the elemental stiffness matrices of Eq. (20) are given as

$$\boldsymbol{D_{tb}} = \sum_{k=1}^{N} \int_{h_k}^{h_{k+1}} [\bar{\boldsymbol{C}}_b^k]\boldsymbol{dz} + \boldsymbol{h_v}[\bar{\boldsymbol{C}}_b^{N+1}] + \boldsymbol{h_p}[\bar{\boldsymbol{C}}_b^{N+2}]$$

$$\boldsymbol{D_{trb}} = \sum_{k=1}^{N} \int_{h_k}^{h_{k+1}} [\bar{\boldsymbol{C}}_b^k][Z_1]\boldsymbol{dz} + \int_{h_{N+1}}^{h_{N+2}} [\bar{\boldsymbol{C}}_b^{N+1}][Z_2]\,\boldsymbol{dz} + \int_{h_{N+2}}^{h_{N+3}} [\bar{\boldsymbol{C}}_b^{N+2}][Z_3]\,\boldsymbol{dz}$$

$$\boldsymbol{D_{rrb}} = \sum_{k=1}^{N} \int_{h_k}^{h_{k+1}} [Z_1]^T \left[\overline{C}_b^k\right][Z_1] dz + \int_{h_{N+1}}^{h_{N+2}} [Z_2]^T \left[\overline{C}_b^{N+1}\right][Z_2]\, dz + \int_{h_{N+2}}^{h_{N+3}} [Z_3]^T \left[\overline{C}_b^{N+2}\right][Z_3]\, dz$$

$$\boldsymbol{D_{ts}} = \sum_{k=1}^{N} \int_{h_k}^{h_{k+1}} [\overline{C}_s^k] dz + h_v[\overline{C}_s^{N+1}] + h_p[\overline{C}_s^{N+2}]$$

$$\boldsymbol{D_{trs}} = \sum_{k=1}^{N} \int_{h_k}^{h_{k+1}} \left[\overline{C}_b^k\right][Z_4] dz + \int_{h_{N+1}}^{h_{N+2}} [\overline{C}_s^{N+1}][Z_5]\, dz + \int_{h_{N+2}}^{h_{N+3}} [\overline{C}_s^{N+2}][Z_6]\, dz$$

$$\boldsymbol{D_{rrs}} = \sum_{k=1}^{N} \int_{h_k}^{h_{k+1}} [Z_4]^T[\overline{C}_s^k][Z_4] dz + \int_{h_{N+1}}^{h_{N+2}} [Z_5]^T[\overline{C}_s^{N+1}][Z_5]\, dz + \int_{h_{N+2}}^{h_{N+3}} [Z_6]^T[\overline{C}_s^{N+2}][Z_6]\, dz$$

$$\left[\boldsymbol{F_{tbp}}\right] = \int_{h_{N+2}}^{h_{N+3}} -\left\{\bar{e}_b^{N+2}\right\}/d_p\, dz\,,$$

$$\left[\boldsymbol{F_{rbp}}\right] = \int_{h_{N+2}}^{h_{N+3}} -[Z_3]^T\left\{\bar{e}_b^{N+2}\right\}/d_p\, dz$$

## REFERENCES

[1] Bailey, T. and Hubbard, J.E., 1985, "Distributed piezoelectric polymer active vibration control of a cantilever beam", J. Guidance, Control and dynamics, Vol. 8, pp. 605–611.

[2] Baz, A. and Poh, S., 1988, "Performance of an active control system with piezoelectric actuators", J. Sound and Vibration, Vol. 126, pp. 327–343.

[3] Hanagud, S., Obal, M.W. and Calise, A.J., 1992, "Optimal vibration control by the use of piezoceramic sensors and actuators", J. Guidance, Control and dynamics, Vol. 15, No.5, pp. 1199–1206.

[4] Ghosh, K. and Batra, R.C., 1995, "Shape control of plates using piezoceramic elements", AIAA Journal, Vol. 33, No. 7, pp. 1354–1357.

[5] Lim, Y.H., Gopinathan, S.V., Varadan, V.V. and Varadan, V.K., 1999, "Finite element simulation of smart structures using an optimal output feedback controller for vibration and noise control", Smart Materials and Structures, Vol. 8, No. 3, pp. 324–337.

[6] Ray, M.C., 2003, "Optimal control of laminated shells with piezoelectric sensor and actuator layers", AIAA Journal, Vol. 41, pp. 1151–1157.

[7] Xu, S.X. and Koko, T.S., 2004, "Finite element analysis and design of actively controlled piezoelectric smart structures", Finite Elements in Analysis and Design, Vol. 40, No. 3, pp. 241–262.

[8] Peng, F., Ng, A. and Hu, Y.R., 2005, "Actuator placement optimization and adaptive vibration control of plate smart structures", J. Intel Mater Syst Struct, Vol. 16, pp. 263–271.

[9] Dong, X.J., Meng, G. and Peng, J.C., 2006, "Vibration control of piezoelectric smart structures based on system identification technique: Numerical simulation and experimental study", Journal of Sound and Vibration, Vol. 297, pp.680-693.

[10] Kwak, M. K., Heo, S. and Jeong, M., 2009,"Dynamic modeling and active vibration controller design for a cylindrical shell equipped with piezoelectric sensors and actuators", Journal of Sound and Vibration, Vol. 321, pp. 510-524.

[11] Foda, M.A., Almajed, A.A. and Eimadany, M.M., 2010, "Vibration suppression of composite laminated beams using distributed piezoelectric patches", Smart Materials and Structures, Vol. 19, 115018.

[12] Mehrabian, A.R. and Yousefi-Koma, A., 2011, "A novel technique for optimal placement of piezoelectric actuators on smart structures", Journal of the Franklin Institute, Vol. 348, pp.12-23.

[13] Baz, A. and Ro, J., 1995, "Optimum Design and Control of Active Constrained Layer Damping", *ASME Journal of Vibrations and Acoustics*, Vol. 117B, pp. 135-144.

[14] Chantalakhana, C. and Stanway, R., 2001, "Active constrained layer damping of clamped–clamped plate vibrations", Journal of Sound and Vibration, Vol. 241, No.5, pp.755–777.

[15] Ro, J. and Baz, A., 2002, "Optimum placement and control of active constrained layer damping using modal strain energy approach", Journal of Vibration and Control, Vol. 8, pp. 861–876.

[16] Ray, M.C. and Reddy, J.N., 2004, "Optimal control of thin circular cylindrical shells using active constrained layer damping treatment", Smart Materials and Structures, Vol.13, pp.64-72.

[17] Bent, A.A. and Hagood, N.W., 1997, "Piezoelectric fiber composites with interdigitated electrodes", Journal of Intelligent Material Systems and structures, Vol. 8, pp. 903-919.

[18] Ray, M. C., 2003, "Optimal Control of Laminated Shells with Piezoelectric Sensor and Actuator Layers", *AIAA Journal*, Vol. 41, pp. 1151-1157.

[19] Kwak, M. K., Heo, S. and Jeong, M., 2009,"Dynamic modelling and active vibration controller design for a cylindrical shell equipped with piezoelectr ic sensors and actuators", Journal of Sound and Vibration, Vol. 321, pp. 510-524.

[20] Sheng, G.G. and Wang, X., 2009, "Active control of functionally graded laminated cylindrical shells", Composite Structures, Vol. 90, pp. 448-457.

[21] Balamurugan, V and Narayanan, S., 2010,"Finite element modeling of stiffened piezolaminated plates and shells with piezoelectric layers for active vibration control, Smart Materials and Structures, Vol. 19, 105003.

[22] Reddy, J. N., Mechanics of Laminated Composite Plates: Theory and Analysis, CRC Press, Boca Raton, FL. 1997.

[23] Kar-Gupta, R. and Venkatesh, T.A., 2007, "Electromechanical response of 1-3 piezoelectric composites: An analytical model", Acta Materialia, Vol. 55, pp. 1093-1108.

[24] Reddy, J.N. and Liu, C.F., 1985, "A higher order shear deformation theory of laminated elastic shells", International Journal of Engineering Sciences, Vol. 23, No. 3, pp. 319-330.